When seeing is not believing

Petrovskaya, Natalia; Zhang, Wenxin

DOI:
10.1016/j.jtbi.2019.110141

Document Version
Peer reviewed version

Citation for published version (Harvard):
Petrovskaya, N & Zhang, W 2020, 'When seeing is not believing: comparative study of various spatial distributions of invasive species', *Journal of Theoretical Biology*, vol. 488, 110141. https://doi.org/10.1016/j.jtbi.2019.110141

When Seeing Is Not Believing: Comparative Study of Various Spatial Distributions of Invasive Species

Natalia Petrovskaya [a1], Wenxin Zhang [a]

[a] School of Mathematics, University of Birmingham, Birmingham, UK.

Abstract

We address the problem of pattern recognition and comparison when spatial patterns of biological invasions are studied. A model of biological invasion is employed to simulate spatio-temporal dynamics of invasive species and generate a variety of spatial patterns including so called 'no front' patchy spatial distributions. We introduce several topological indices to understand whether various spatial distributions of invasive species can be compared to each other based on information about their topology. We also investigate how topological indices used to make conclusions about the spatial pattern are related to controlling parameters in the underlying process of biological invasion. Our analysis reveals that a small increment in the model parameters results in a small increment in topological indices when the topology of continuous front spatial pattern with no patches behind the front is considered. Meanwhile, no front patchy spatial distributions present a different case where a small change in the model parameters results in random fluctuations of topological indices. The 'random' behaviour of patchy patterns is further studied to understand whether a patchy spatial structure can transform itself into a continuous front spatial distribution over time. In the paper it will be argued that apart the topological quantities used to classify spatial distributions, the transition time required to establish topological properties of the spatial pattern must be taken into account in pattern recognition and analysis. Furthermore, it will be demonstrated that for some parameter values it is impossible to conclude about the topological type of spatial pattern, i.e. continuous front spatial distributions cannot be distinguished from 'no front' patchy distributions of invasive species, no matter what their topological indices are.

Keywords: biological invasion, spatial pattern, pattern recognition, patchy spread, transient regime

[1]Corresponding author. Email: n.b.petrovskaya bham.ac.uk

1 Introduction

Understanding the properties of the spatio-temporal patterns of alien species spread during biological invasion is a problem of considerable theoretical and practical importance as it has implications for the management and control of invasive species [26, 60]. The seminal results in the theory of biological invasion obtained in [9], [22] and [57] have stated the existence of a continuous population front separating an invaded area behind the front from a non-invaded area. Furthermore, complex spatial structures such as isolated population colonies may appear in the wake of the invasion front [53, 54] and beyond the population front[52, 56].

However, in recent decades, an alternative hypothesis of 'patchy' invasion has emerged. This 'patchy' invasion regime implies the alien species spread occurs entirely through the formation and dynamics of isolated patches of high population density observed everywhere in the domain in the absence of any continuous front [32, 34, 45, 47, 50]. The mathematical theory of 'no front' patchy invasion is not well developed and is still unclear how patchy spatial patterns may differ from continuous front patterns from a topological viewpoint. Agglomeration of separate patches located close to each other may look like a continuous front spatial distribution and simple visual inspection of those patterns may easily result in a wrong conclusion about the type of biological invasion (cf. spatial structures in Fig. 1a and Fig. 1b). The situation is further exacerbated by the fact that the formation of no front patchy structures is possible for many invasion regimes generated in simulation, yet in many cases transition from continuous front to patchy patterns and vice versa cannot be predicted when parameters in the model used to simulate biological invasion are varied (e.g. see [19, 43]). Thus, a question arises about reliable criteria to allow one to compare the topology of continuous front and patchy spatial structures. Elaboration of such criteria should, in turn, help practitioners to design more efficient monitoring and control protocols to deal with invasive species [60].

The importance of accurate classification and quantification of ecological patterns has been acknowledged by scientists since long ago [12, 24, 16] and developing reliable and efficient methods for analysing spatial pattern remains an important stream of research in ecology [3, 10, 23, 40]. Various approaches have been employed (e.g. see [5, 51] and references therein) and there is ongoing research to combine multiple spatial pattern analysis techniques into a single paradigm [4, 29]. The methods of pattern recognition are of great demand in the problem of biological invasion [8, 29, 31, 58], yet a universal protocol for spatial pattern analysis does not exist and criteria for comparison between continuous front spatial structures and discontinuous spatial distributions remain unclear. Primary topological analysis of 'no front' patchy spatial patterns in a specific model of patchy invasion has been carried out in [43, 44]. In this paper we utilize the approach in [44] to investigate several topological characteristics that can potentially help us to compare various spatial structures.

The simplest, yet reliable, way to distinguish between the continuous front and patchy spatial patterns is based on counting the number of objects in the image of spatial distribution [43]. Any continuous front is considered as a single object, while a 'no front' patchy structure can be thought of as several separate objects in the spatial domain. However, given that continuous front spatial pattern may have a complex patchy spatial structure behind the front,

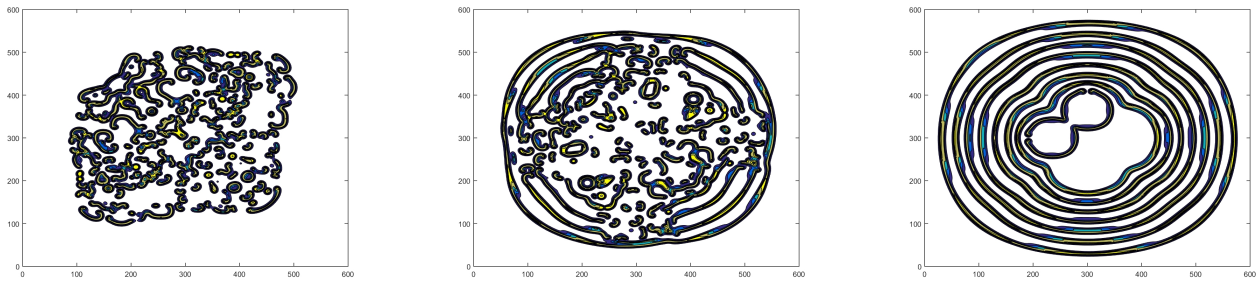

(a) (b) (c)

Figure 1: *Are these spatial patterns similar or different? (a) Patchy spatial distribution of the density of invasive species obtained as a result of numerical solution of the mathematical model of biological invasion (see Section 2); (b) Continuous front density distribution obtained from the same model. The spatial pattern has a patchy structure behind the front. (c) Continuous front density distribution with quasi-regular oscillations behind the front.*

a more careful analysis of topological properties may be required. Consider, for example, the spatial patterns in Fig. 1. Is the spatial pattern in Fig. 1b similar to the spatial distribution in Fig. 1a, as the pattern in Fig. 1b has similar patchy structure behind the front? On the other hand, is the pattern of Fig. 1b topologically closer to a spatial distribution of Fig. 1c because both of them are continuous fronts? The above questions cannot be answered unless some problem-specific topological indices are introduced to decide to what extent two spatial distributions are similar to each other.

We focus our attention on the spatial data obtained in simulations as we need to analyse plenty of images of spatial patterns produced with high resolution. Field data related to patchy invasion are not readily available to meet the requirements of our study. Hence we employ a reaction-diffusion model to simulate spatio-temporal dynamics of biological invasion. The model has previously been investigated in [47] where its capacity to generate a variety of spatial patterns has been demonstrated. In particular, we are interested in spatial distributions looking similar to each other while spatial pattern analysis reveals that some of them are continuous fronts while the others are patchy spatial patterns where no continuous front exists. We aim to investigate whether any reliable criteria can be proposed to distinguish between those distributions. Basic topological indices of the spatial pattern (the number of objects, the fragmentation rate, etc.) will be employed to see if the spatial pattern type can be recognised correctly by using any of the quantities above.

Once topological indices have been selected and calculated to quantify spatial patterns the next question we are concerned with is how these indices respond to a change in the model parameters. This question is of considerable interest because it contributes to the discussion on whether the process responsible for spatial pattern formation can be at least partly understood by pattern analysis on its own [20, 31]. Consider again the spatial patterns in Fig. 1. One approach to make conclusions about similarity of these spatial distributions would

be to compare their topology by calculating several topological indices. Meanwhile, another approach would be to compare the model parameters resulting in the generation of spatial patterns in the figure and state that two patterns are similar if they are produced from the same model with close values of parameters. Parameters of the underlying process responsible for the formation of certain spatial patterns are often unknown when field data are analysed. However, since we use a well-defined mathematical model to generate spatial distributions, it can be readily verified whether spatial patterns with close values of the topological indices correspond to close values of the model parameters. If the latter statement is true then information about model parameters required to generate a spatial pattern with certain topological properties, i.e. continuous front or 'no front' patchy spatial distribution, can be obtained from the analysis of existing spatial patterns. Hence, it will be investigated in the paper whether the spatial patterns produced for slightly differing model parameters have similar topological indices. Our analysis reveals that a small increment in the model parameters results in a small increment in topological indices when the topology of a continuous front that has no patches behind the front is considered. The above conclusion, however, does not hold when we analyse continuous front density distributions that have patchy patterns behind the front and, most of all, spatial distributions consisting of separate patches. In the latter case, a small change in the model parameters results in random fluctuations of topological indices as a spatial pattern with very different topology may appear.

Since patchy spatial structures have different topological indices even when they are produced by the same model with close parameter values the question about 'topological stability' of those spatial structures arises. The 'random' behaviour of patchy patterns is further studied in the paper to understand whether a patchy spatial structure can transform itself into a continuous front spatial distribution as time progresses. We argue that information about the spatial pattern alone is not sufficient to conclude the type of spatial distribution (i.e. patchy pattern vs. continuous front) and spatio-temporal dynamics must be taken into account when formation and propagation of patchy structures are considered.

The paper is organized as follows. In the next section, we briefly formulate a mathematical model of biological invasion used to generate various spatial distributions of the population density. In Section 3, we employ several topological indices for classification of spatial patterns. We show that, while those indices are reliable for the analysis of topologically simple spatial structures, we cannot use them for the comparison of patchy spatial distributions. We then study spatio-temporal dynamics of invasive species in Section 4 and demonstrate that random variations in the topological indices persist as time progresses when topologically complex patchy patterns are considered. Moreover, propagation of the invasive species can be 'topologically unstable', i.e. spatial distribution can experience random switches between continuous front spatial distributions and 'no front' patchy spatial distributions over the time we are interested in. Finally, Section 5 provides discussion and concluding remarks.

2 Model and method

The standard reaction-diffusion framework that can be employed for the simulation of biological invasion is [2, 35, 55, 53]

$$\frac{\partial U(X,Y,T)}{\partial T} = D_U\left(\frac{\partial^2 U}{\partial X^2}+\frac{\partial^2 U}{\partial Y^2}\right)+F(U,V), \quad (1)$$

$$\frac{\partial V(X,Y,T)}{\partial T} = D_V\left(\frac{\partial^2 V}{\partial X^2}+\frac{\partial^2 U}{\partial Y^2}\right)+G(U,V). \quad (2)$$

where $U(X,Y,T)$ and $V(X,Y,T)$ are the population densities of two interacting species at time $T>0$ and position (X,Y). Depending on the problem, those species may be thought of as prey and predator, host and parasite, herbivore and grazer [54]. Coefficients D_U and D_V describe species diffusivity due to the movement of the individuals. The local dynamics $F(U,V)$ and $G(U,V)$ are defined to accommodate the properties of particular species.

For our study, the main criterion for selection of functions $F(U,V)$ and $G(U,V)$ is that the spatio-temporal dynamics can produce both continuous front and 'no front' patchy spatial distributions. Thus we adopt the definition of local dynamics considered previously in [47] where it has been demonstrated that their model modified after [36] to include the Allee effect is capable of generating the wealth of spatial distributions including 'no front' spatial structures. The model is formulated within the susceptible-infective framework where the invasive species has been handled as a susceptible population whose spread is controlled by the pathogen. The spatio-temporal dynamics of the invasive species in (1–2) is then given by

$$\frac{\partial U(X,Y,T)}{\partial T} = D\left(\frac{\partial^2 U}{\partial X^2}+\frac{\partial^2 U}{\partial Y^2}\right)+P(U)-E(U,V), \quad (3)$$

$$\frac{\partial V(X,Y,T)}{\partial T} = D\left(\frac{\partial^2 V}{\partial X^2}+\frac{\partial^2 U}{\partial Y^2}\right)+E(U,V)-MV. \quad (4)$$

Here U and V in (3–4) are the densities of the susceptible and infected population, respectively, the function $E(U,V)$ describes disease transmission, $P(U)$ describes the local population growth where infected individuals do not contribute to the growth rate (as the disease is terminal) and M is the mortality rate for the infected population. We assume that the diffusivity coefficients are $D_U = D_V = D$ for the sake of simplicity. The growth rate P is selected as to incorporate the strong Allee effect into the model (e.g. see [6, 28]):

$$P(U) = \left(\frac{4\nu}{(K-U_0)^2}\right)U(U-U_0)(K-U), \quad (5)$$

where parameter K is the carrying capacity of the susceptible population, U_0 is the Allee threshold density ($0<U_0<K$), ν is the maximum per capita growth rate (cf. [25]). The transmission function E is considered in the form of the mass-action law

$$E(U,V) = AUV, \quad (6)$$

where A is the rate of infection transmission. We consider the population dynamics in a square-shaped domain Ω of size L, so that $0 < X < L$ and $0 < Y < L$. At the domain boundary $\partial\Omega$ the zero-flux conditions are used.

To obtain the population distributions, the system (3–4) is solved numerically by implementing a finite difference method. For convenience, we first introduce dimensionless variables. The carrying capacity K makes a convenient scale for the population density, $u = U/K$ and $v = V/K$. We also introduce parameter $a = AK$ to make the coordinates $x = X(a/D)^{1/2}$ and $y = Y(a/D)^{1/2}$ and the dimensionless time is $t = aT$. Equations (3)–(4) then take the following form:

$$\frac{\partial u(x,y,t)}{\partial t} = \left(\frac{\partial^2 u}{\partial x^2} + \frac{\partial^2 u}{\partial y^2}\right) + \gamma u(u-\beta)(1-u) - uv \ , \tag{7}$$

$$\frac{\partial v(x,y,t)}{\partial t} = \left(\frac{\partial^2 v}{\partial x^2} + \frac{\partial^2 v}{\partial y^2}\right) + uv - mv \ , \tag{8}$$

where $\beta = U_0/K < 1,\ \gamma = 4\eta K(A(K-U_0))^2,\ m = M/a$ are dimensionless parameters.

The boundary conditions are

$$\frac{\partial u}{\partial \mathbf{n}} = 0 \quad \text{and} \quad \frac{\partial v}{\partial \mathbf{n}} = 0,$$

where $\mathbf{n}$ is the outward unit normal vector to boundary $\partial\Omega$.

The initial distribution we use in the problem is as follows:

$$\begin{aligned} &u(x,y,0) + v(x,y,0) = 1, \quad \text{for } |x - L/2| < l_u,\ |y - L/2| < l_u, \\ &u(x,y,0) + v(x,y,0) = 0, \qquad\qquad\qquad otherwise, \end{aligned} \tag{9}$$

i.e. the population is considered to be homogeneously distributed at its carrying capacity within a square area of size l_u , $0 < l_u < L/2$. We also assume that the infested population is initially concentrated in a smaller domain

$$\begin{aligned} &v(x,y,0) = \kappa, \quad \text{for } |x - L/2| < l_v,\ |y - L/2| < l_v, \\ &v(x,y,0) = 0, \qquad\qquad\qquad otherwise, \end{aligned} \tag{10}$$

where $0 < l_v \le l_u$ and $\kappa \le 1$. We assume symmetric initial conditions, i.e. both subdomains of size l_u and l_v are placed at the center of the domain as specified in (9)-(10) (but cf. spatial density distributions $u(x,y)$ in Fig. 1 obtained from asymmetric initial conditions). One reason we want to use the symmetric initial conditions is that the numerical solution remains symmetric at any time $t > 0$ and the solution symmetry can then be considered as a reliable means to control the accuracy of the numerical method. Meanwhile, it is worth mentioning here that basic topological properties of spatial patterns are not affected by the choice of asymmetric initial conditions although their qualitative estimates are, of course, different; see also the discussion in [43] where the sensitivity of the results to the choice of the initial conditions has been investigated.

2.1 Stability of the non-spatial problem

For the rest of this paper, we are interested in spatial distributions of the density $u(x, y)$ of the susceptible population of invasive species obtained as a result of the numerical solution to equations (7-8) with initial conditions (9-10). Since the topological analysis of spatial patterns requires us to deal with a variety of spatial distributions we must have a well-informed guess about the parametric range related to the formation of 'no front' patchy patterns. Our inference based on the analysis made for other relevant models (e.g. [32, 47]) is that the patchy invasion is likely to occur for parameters where the only attractor in the non-spatial system is the extinction state. Hence our next step is to investigate a non-spatial counterpart of the system (7-8) given by

$$\frac{du(t)}{dt} = \gamma u(u-\beta)(1-u) - uv, \tag{11}$$

$$\frac{dv(t)}{dt} = uv - mv. \tag{12}$$

The demographic parameters m and β determine steady states of (11-12), i.e. the extinction state $s_1 = (0, 0)$, two susceptible-only states $s_2 = (1, 0)$ and $s_3 = (\beta, 0)$, and the coexistence state $s_4 = (m, \gamma(m-\beta)(1-m))$. While the steady states s_1, s_2, and s_3 always exist, the coexistence state s_4 is feasible for $m < 1$ and $\beta < m$.

The linear stability analysis requires computation of the eigenvalues λ_1 and λ_2 of the linearised system,

$$\lambda_{1,2} = \frac{1}{2}\left(tr(\mathbf{J}) \mp \sqrt{tr(\mathbf{J})^2 - 4det(\mathbf{J})}\right), \tag{13}$$

where $tr(\mathbf{J})$ and $det(\mathbf{J})$ are the trace and the determinant of the Jacobian matrix $\mathbf{J}$ of (11-12) taken at the corresponding steady state s_i, $i = 1, \ldots, 4$. Computation of eigenvalues (13) reveals that λ_1 and λ_2 are real numbers when computed at steady states s_1, s_2 and s_3. The stability analysis concludes that s_1 is always stable, s_2 is stable for $m > 1$ and $\beta < 1$, and the steady state s_3 is only stable when $\beta > m$ and $\beta > 1$, i.e. for the range of β where s_3 is unfeasible.

The eigenvalues λ_1 and λ_2 computed at the coexistence state s_4 are given by (13) where $tr(\mathbf{J}) = \gamma m(1 - 2m + \beta)$ and $det(\mathbf{J}) = m\gamma(m-\beta)(1-m)$. Let us introduce function $F(\beta)$ as

$$F(\beta) \equiv tr(\mathbf{J})^2 - 4det(\mathbf{J}) = \gamma^2 m^2(\beta - 2m + 1)^2 - 4\gamma m(\beta - m)(m-1).$$

To find sub-domains in the parametric plane (m, β) where the eigenvalues $\lambda_{1,2}$ are complex numbers we factorise $F(\beta) = (\beta - \beta_1(m))(\beta - \beta_2(m))$. We have

$$\beta_{1,2}(m) = 2m - 1 + \frac{2(m-1)}{\gamma m}\left(1 \mp \sqrt{\gamma m + 1}\right).$$

The structure of the parameter plane (m, β) is shown in Fig. 2a where the curves $\beta_1(m)$ and $\beta_2(m)$ are shown for $m > 0$ and $\beta > 0$ as two dashed lines in the figure. We have $\beta_1(m) > \beta_2(m)$ for $0 < m < 1$ and $\beta_1(m) < \beta_2(m)$ for $m > 1$. Thus $F(\beta) < 0$ in sub-domains where $m < 1$, $\beta_2(m) < \beta < \beta_1(m)$ and $m > 1$, $\beta_1(m) < \beta < \beta_2(m)$, respectively. The

eigenvalues $\lambda_{1,2}$ are complex numbers in those sub-domains and the temporal dynamics is oscillatory. Further analysis reveals that the coexistence state s_4 is unstable when $tr(J) > 0$ i.e. $\beta > 2m - 1$.

Note that $\beta_1(m) > 0$ for $m > 0$ and the only positive root $m^* > 0$ of function $\beta_2(m)$ is given by

$$m^* = \frac{\gamma - 1 + \sqrt{2\gamma + 1}}{2\gamma}.$$

Thus, the location of root m^* and therefore the size of the domain $\beta_2(m) < \beta < \beta_1(m)$ depends on parameter γ where the asymptotic limits are $m^*(\gamma) \to 1$ as $\gamma \to 0$ and $m^*(\gamma) \to 1/2$ as $\gamma \to \infty$.

We now return to the spatio-temporal problem (7-8). Based on the analysis of the non-spatial system (11-12) and the results of previous work [34, 45, 47] we may expect that for any fixed value of γ patchy spatial patterns will arise when parameter m is chosen along the line $\beta = const$ in the 'transitional' zone between the extinction state (the region $\beta > m$) and the stable coexistence state (the region $\beta < 2m - 1$). The above guess is further confirmed by computation and topological analysis of spatial distributions. A fragment of the parametric plane (m, β) along with the solution type obtained for every pair (m, β) at time $t = 600$ for $\gamma = 6.0$ is shown in Fig. 2b. Pairs (m, β) in the parametric plane resulting in different spatial patterns are color-coded in the figure as blue stars for the extinction, red triangles for patchy invasion (no continuous front), green circles for continuous front spatial distributions.

Let us fix the value of β and decrease parameter m as we move along the line $\beta = const$ in

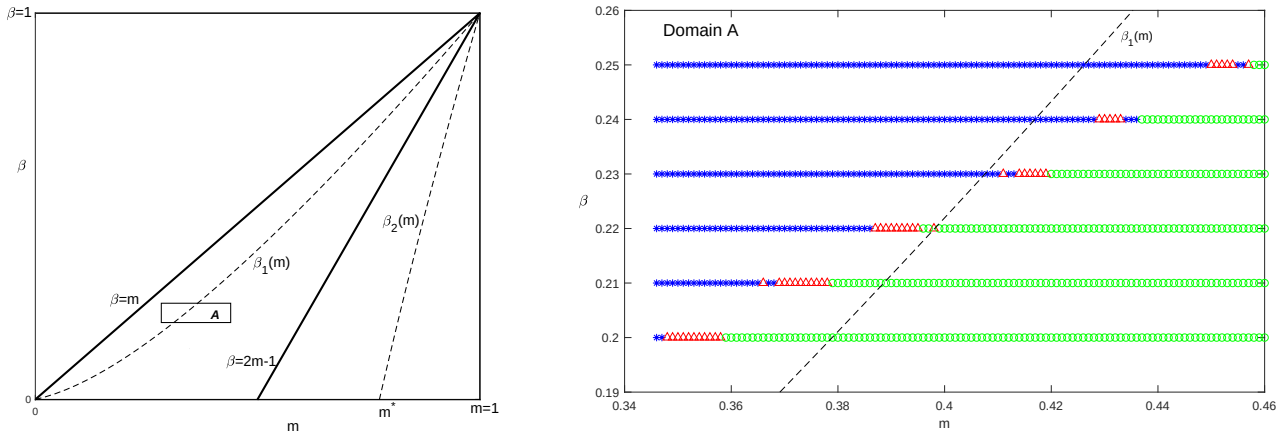

(a) (b)

Figure 2: *(a) The parametric plane (m, β) for non-spatial equations (11-12). (b) Various spatial patterns obtained in numerical solution of the spatial system (7-8) at time $t = 600$. Parameters m and β are taken in the Domain A (see Fig. 2a) of the parametric plane and are varied with a small increment, parameter $\gamma = 6.0$. Pairs (m, β) in the parametric plane resulting in different spatial patterns are color-coded as follows: blue stars for the extinction, red triangles for patchy invasion (no continuous front), green circles for continuous front spatial distributions.*

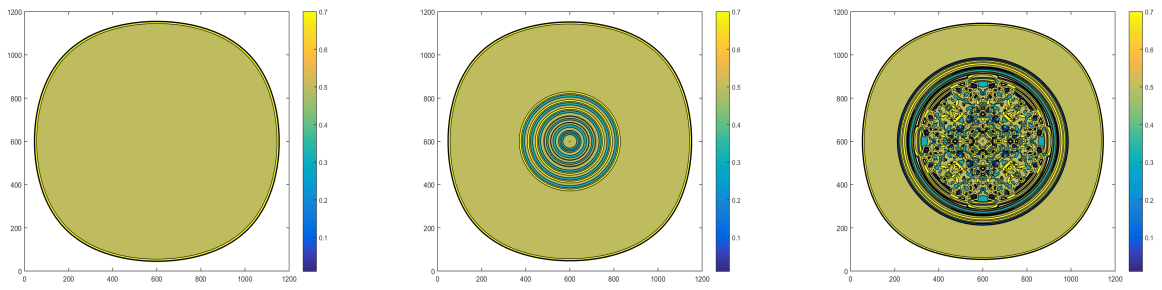

(a) (b) (c)

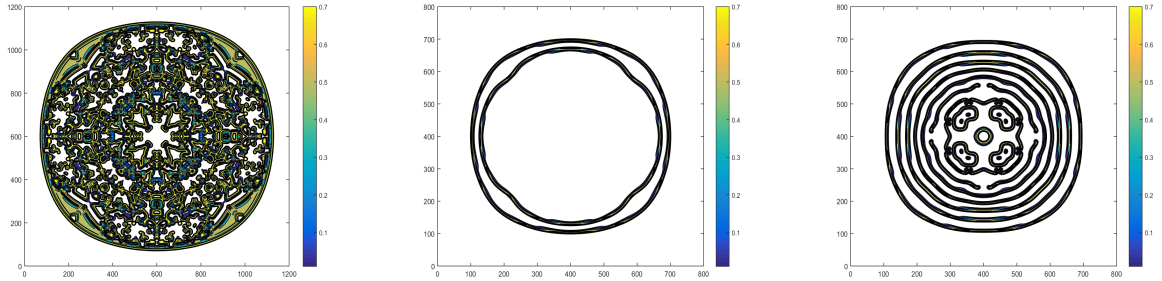

(d) (e) (f)

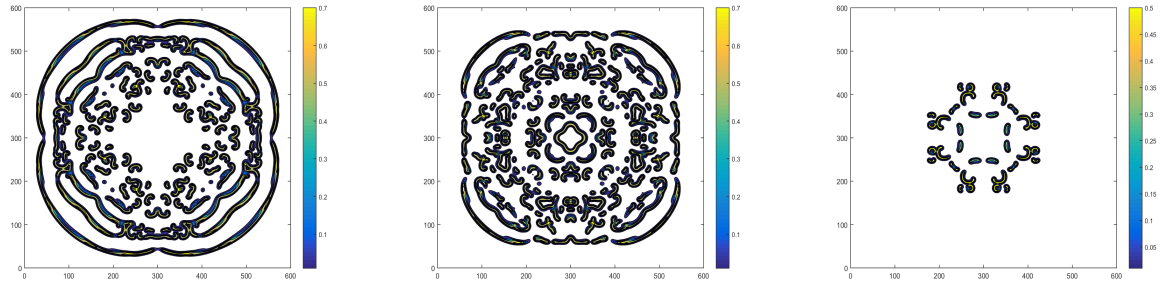

(g) (h) (i)

Figure 3: *Basic spatial patterns arising in the model (7-8) (see also Fig. 2b). Snapshots of the spatial density distribution obtained for various values of parameter m at time $t = 600$. The other problem parameters are $\beta = 0.21$ and $\gamma = 6.0$. The white colour in each panel corresponds to zero populaiton density (not shown in the figure legend). (a) $m = 0.600$: continuous front with no oscillations in the front wake; (b) $m = 0.59$: continuous front with regular oscillations in the front wake; (c) $m = 0.57$: continuous front with irregular oscillations in the wake; (d) $m = 0.53$: irregular oscillations become more distinct in the wake; (e) $m = 0.38675$: irregular oscillations in the wake are located in a narrow domain close to the front; (f) $m = 0.3860$: continuous front with patchy pattern formation in the wake; (g) $m = 0.379$: a patchy pattern in the wake of continuous front becomes more distinct as m decreases; (h) $m = 0.378$: continuous front breaks down as m further decreases; (i) $m = 0.366$: a patchy pattern consisting of few separate patches appears before the population becomes extinct at smaller values of parameter m.*

the parametric plane of Fig. 2b. Basic spatial distributions obtained in the numerical solutions of the model (7-8) when m is varied are shown in Fig. 3. All spatial patterns in the figure have been generated for $\beta = 0.21$ and $\gamma = 6.0$ at time $t = 600$. The size of the computational domain has been varied under the requirement that the invasive species must not approach the domain boundary at $t = 600$ (areas with zero population density are shown in white in the figure). A convex continuous front in Fig. 3a obtained for $m = 0.60$ presents the simplest pattern from a topological viewpoint and we should expect similar spatial distributions for $m > 0.60$. Meanwhile, as we slightly decrease m to 0.59 regular oscillations appear in the front wake; see Fig. 3b. Further decrease in m results in irregular oscillations in the wake as shown in Fig. 3c obtained for $m = 0.57$. Those irregular oscillations become stronger at smaller values of parameter m; see Fig. 3d where $m = 0.53$. For smaller values of m, the topology of spatial pattern changes again as all oscillations are now located at a narrow ring-shaped spatial domain close to the front as shown in Fig. 3e obtained for $m = 0.38675$; the visual image of the spatial distribution might appear confusing yet the presence of oscillations is indicated by the density range in the legend. The spatial distribution in the wake then breaks down as m decreases and the formation of patches occurs behind the front as shown in Fig. 3f with $m = 0.3860$. The patchy pattern in the wake of the continuous front becomes then more distinct as m decreases; see Fig. 3g obtained for $m = 0.379$. If we further decrease the value of m a continuous front breaks down and the topology of spatial pattern undergo another significant change as spatial patterns will appear as a collection of separate patches of the non-zero density. One example of patchy spatial distribution is shown in Fig. 3h for $m = 0.378$ (cf. Fig. 2b). Further evolution of the patchy pattern as m decreases can be seen in Fig. 3i where the spatial pattern obtained for $m = 0.366$ now consists of few separate patches with no resemblance to continuous fronts in Figs. 3a–3e. Finally, the population becomes extinct when $m < 0.365$; cf. the results in Fig. 2b.

In the present paper, we are mostly interested in the topological analysis of patchy spatial patterns and we, therefore, consider the range of parameter m where patches appear either in the wake of continuous front or as separate topological structures. That 'patchy' range of m depends on parameters β and γ in the model (cf. Fig. 2b) and it can be approximately identified as $m \in [0.365, 0.386]$ for $\beta = 0.21$ and $\gamma = 6.0$ (a more accurate definition of the 'patchy' range will be provided in Section 4).

The wealth of spatial patterns arising in the model cannot be classified by simple visual inspection only. Moreover, the visual comparison of Fig. 3g and Fig. 3h leads us to the conclusion that continuous front spatial patterns may not always be easily distinguished from patchy patterns. Hence in the next section, we introduce several rigorous topological characteristics of spatial patterns to provide an accurate comparison of continuous and patchy spatial distributions based on their topological indices.

3 Topological indices of spatial patterns

We follow our previous study in [43, 44] where we have analysed various spatial structures appearing when a system of integro-difference equations is solved to simulate the propagation of invasive species into the space under the assumption of a certain type of spatial dispersal. Although the analysis of spatial patterns has been done in [43, 44] for a different model of biological invasion, topological indices used there are general enough to be applied to spatial patterns arising in the model (7–8). We also note that all the topological indices we employ to study spatial patterns can be calculated directly from the spatial population density $u(x, y)$ and there is no need to use advanced statistical methods designed to evaluate topological indices from discrete spatial data such as trap counts or individual positions (cf. [39, 48]).

Below we introduce the basic topological indices employed to study spatial patterns.

3.1 The number of objects and the density of objects

An object in the image of the spatial density distribution $u(x, y)$ is defined as a region of the non-zero spatial density[2] with a closed external boundary. The number of objects n in the image of spatial pattern is a key characteristic of the pattern as it defines the pattern type. Namely, a continuous front density distribution can be classified as a single object (i.e. we have $n = 1$), where any patchy density distribution in the front wake is ignored. For instance, each of the spatial patterns in Fig. 3f and Fig. 3g presents a single object, no matter how complex the topological structure behind the front is in those density distributions. Meanwhile, a 'no front' patchy spatial distributions in Fig. 3h and Fig. 3i are considered as a collection of separate objects in a spatial domain, where every patch counts as a single object (i.e. $n > 1$).

The number of objects in the image of a spatial density distribution is calculated with the help of the Image Processing Toolbox (IPT) in MATLAB [30]; see also [43] where the computational procedure is explained in detail. Using the IPT software allows us to count the number of objects n in any image of spatial density $u(x, y)$, no matter how topologically complex the spatial pattern is. We can, therefore, proceed with a more refined study of the parametric plane in Fig. 2b and check the 'degree of patchiness', i.e. the number of separate patches in every patchy distribution. That, in turn, will allow us to conclude about the similarity of spatial patterns generated for pairs (m, β) chosen close to each other in the parametric plane, i.e. to see whether those spatial patterns have a similar number of objects.

Let us vary the value of parameter m when we move along the line $\beta = 0.21$ in the parametric plane of Fig. 2b. We compute the number of objects n for each spatial distribution obtained at time $t = 600$ when $m \in [0.362, 0.396]$ where the parametric sub-domain resulting in patchy spatial patterns is of particular interest. The graph $n(m)$ is shown in Fig. 4a where we assume that $n = 0$ corresponds to the extinction regime (i.e. no objects in the spatial domain). It is obvious from the graph that using topological index n readily allows for the recognition of the 'patchy' sub-domain in the parametric plane as $n > 1$ for $m \in [0.365, 0.379]$.

[2]In our model we consider $u(x, y) = 0$ in the image processing routine if we have $u(x, y) < \epsilon = 10^{-6}$ in the numerical solution.

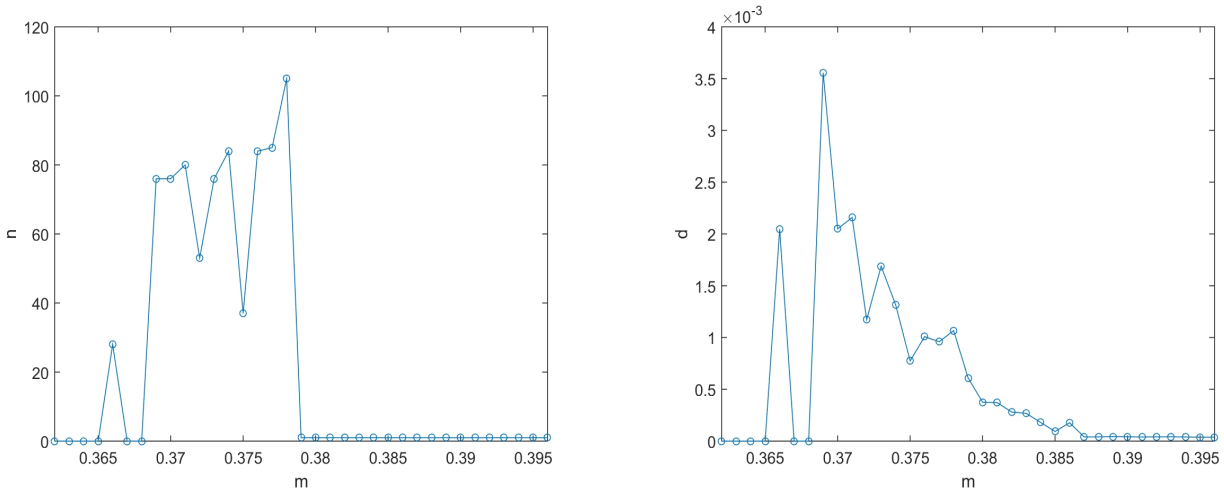

(a) (b)

Figure 4: *Topological indices of spatial patterns as a function of parameter m in the model (7)–(8) with the initial conditions (9)–(10) and parameters $\beta = 0.21$, $\gamma = 6.0$. The spatial distributions have been obtained for various m at time $t = 600$. (a) the number of objects, $n(m)$; (b) the density of objects, $d(m)$.*

It is also seen from the graph that the number of objects occasionally varies for values of m resulting in the formation of patchy patterns as a small increment in m results in a random up- or down-jump in $n(m)$ in the sub-domain $m \in [0.365, 0.379]$. It has been checked in our computation that a similar conclusion about random variation in $n(m)$ over the interval of m responsible for patchy patterns can be made when another line $\beta = const$ is chosen in the parametric plane of Fig. 3b, although we do not show those results for the sake of brevity. Thus the number of objects is a reliable index when the identification of patchy patterns is required yet the knowledge of n does not allow us to conclude about the similarity of patchy patterns as spatial distributions obtained for close values of parameter m may have a very different number of objects.

The number of objects is a key topological index if we want to distinguish between the continuous front and patchy patterns. That index, however, does not take into account a fine topological structure of the spatial pattern. This is especially true for complex patterns in the wake of the continuous front where the number of patches behind the front can be very high (e.g. see Fig. 3g) yet the number of objects remains $n = 1$. One straightforward approach to analyse spatial structures behind the front would be to use the density of objects. The density of objects d has been defined in [44] as

$$d = \frac{\tilde{n}}{A}, \tag{14}$$

where $\tilde{n}$ is now the total number of objects in the image (including all objects behind the continuous front), and A is the total area occupied by those objects.

Let us investigate how the density of objects depends on the parameter m and compute d for spatial patterns generated for the range of m in Fig. 4a where the number of objects has previously been found. The graph $d(m)$ is shown in Fig. 4b. It is seen from the graph that topological index d changes significantly when transition occurs from one topological type of spatial pattern to another type. While the density of objects remains constant for $m > 0.386$ (no patches behind the front), it keeps growing when m decreases from $m = 0.386$ to $m = 0.379$ (patterns with patchy structure behind the front). Meanwhile, a predictable conclusion drawn from definition (14) along with the graph $n(m)$ in Fig. 4b is that we cannot compare various patchy distributions to each other based on their density of objects. The density of objects experiences random jumps in the value of d when $m \in [0.365, 0.379]$, i.e. when m is in the parametric sub-domain corresponding to the formation of patchy patterns and patterns with close values of m may have different density of objects d.

3.2 The Morisita index and the fragmentation rate

We now want to proceed with further classification of a fine topological structure of spatial patterns where we aim to find topological indices that could help us to distinguish between various patchy distributions. Among the other indices used in statistical ecology to quantify spatial patterns (e.g. see [17] and references therein) the Morisita index [33] has been widely used in various ecological studies to decide about the degree of aggregation in spatial distribution [1, 7, 15, 18]. The Morisita index I_M is defined as

$$I_M \;=\; Q\,\frac{\sum_{k=1}^{Q} n_k(n_k-1)}{N(N-1)}, \tag{15}$$

where N is the total number of 'population units' whose definition depends on a particular problem under consideration and will be explained later in the text, Q is the number of quadrats (i.e. the number of auxiliary sub-domains used to count the 'population units') and n_k is the number of 'population units' in the kth quadrat. The Morisita index provides a simple and convenient measure of how likely it is that two randomly selected individuals in a given distribution are found within the same quadrat compared to that of a uniform random distribution. It can be proved that, if the population is distributed quasi-uniformly over the domain then I_M is always less then the Morisita index calculated when the population of the same size is aggregated in the domain [21].

Consider, for example, two hypothetical patchy spatial distributions shown in Fig. 5a and Fig. 5b where where the black cells represent a population density of 1 and the white cells have a population density of 0. Hence our 'population units' in this example are presented by black cells and we have $N = 12$ in both cases. In our example, we divide the domain into $Q = 4$ quadrats (where each quadrat will contain 16 grid cells) and count the number of population units (i.e. the number of black cells) in each quadrat. The Morisita index does depend on the number Q of quadrats yet it allows one to compare topological properties of various spatial patterns when the number of quadrats in (15) is agreed. The computation of expression (15) for given $Q = 4$ reveals that Morisita index I_M of the spatial patterns in Fig. 5a and Fig. 5b

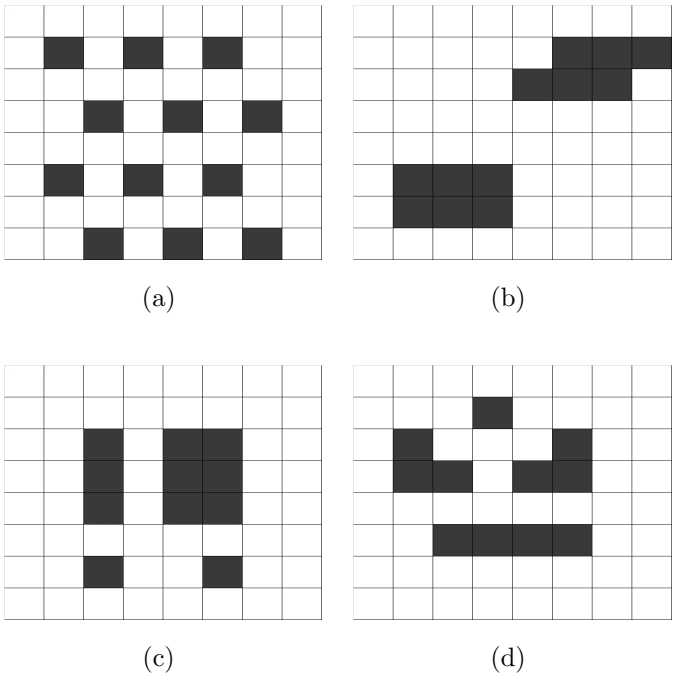

Figure 5: *Hypothetical spatial patterns with different topological indices. (a)-(b) The degree of spatial aggregation in the two patterns measured by the Morisita index is different: (a) quasi-uniform density distribution,* $I_M = 0.73$*; (b) highly aggregated density distribution with the same area of the non-zero density* $I_M = 1.82$*; (c)-(d) The fragmentation rate measures a 'fine' topological structure of spatial distribution. The two spatial patterns have the same area of the non-zero density, the same number of objects, the same Morisita index, but their fragmentation rate is different: (c) The fragmentation rate calculated according to (17) is* $I_{fr} = 0.40$*; (d) the fragmentation rate is* $I_{fr} = 0.53$*.*

is different as their degree of aggregation is different. The quasi-uniform spatial distribution in Fig. 5a has the Morisita index $I_M = 0.73$ while the highly aggregated spatial pattern in Fig. 5b has $I_M = 1.82$ for the same Q value.

Let us go back to problem (7-8) and compute the Morisita index I_M as a function of m for the same parameter range as in Section 3.1. The population units are now defined as grid cells on our computational grid used for the numerical solution of problem (7-8) and we choose the number of quadrants $Q = 18$. The graph $I_M(m)$ is shown in Fig. 6a. The analysis of I_M reveals that the Morisita index allows one to distinguish between topologically different patterns: a sharp jump in the Morisita index at $m = 0.386$ corresponds to topological transition from continuous front patterns with no patches ($m > 0.386$) and a high degree of aggregation to the formation of separate patches behind the front ($m \leq 0.386$) that results in less spatially aggregated patterns; cf. Fig. 3e and Fig. 3g. The Morisita index then becomes almost constant ($I_M \approx 2.1$) at $m \in [0.379, 0.386]$ where spatial patterns are continuous fronts with patches behind the front. Meanwhile, I_M starts increasing when the transition from continuous front to patchy spatial distributions occurs at $m = 0.379$. The spatial pattern appearing at $m = 0.366$

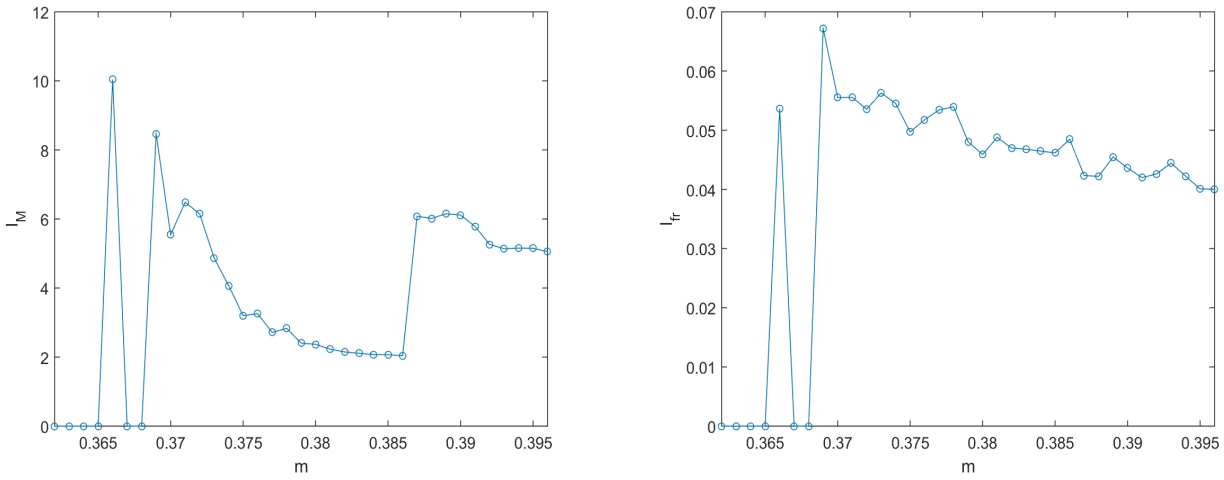

(a) (b)

Figure 6: *Topological indices of spatial patterns as a function of parameter m in the model (7)–(8) with the initial conditions (9)–(10) and parameters $\beta = 0.21$, $\gamma = 6.0$, $t = 600$. (a) the Morisita index, $I_M(m)$; (b) the fragmentation rate, $I_{fr}(m)$.*

before the transition to the extinction sub-domain $m \leq 0.365$ has the highest Morisita index $I_M = 10.1$ as the image consists of a small number of patches (cf. Fig. 3i) which is considered as a high degree of aggregation according to definition (15). However, despite the Morisita index showing a trend to grow as m decreases in the 'patchy' parametric sub-domain, we notice several occasional jumps in I_M when m varies in the 'patchy' range.

The last topological index we discuss in this section is fragmentation rate I_{fr}. Although the fragmentation rate can loosely be thought of as a quantity inverse to Morisita index I_M, it cannot be entirely replaced by the latter quantity. Consider, for example, two spatial distributions shown in Fig.5c and Fig.5d. The number of objects $n = 4$ is the same in both patterns and the area occupied by each spatial distribution is the same in Fig.5c and Fig.5d and is equal to 12 units where we consider the area of any square cell equal to one. Moreover, the Morisita index is the same for both patterns and is equal to 0.8. The patterns, however, are different and another, more 'subtle' topological index is required to recognise that difference. We, therefore, introduce the fragmentation rate of the spatial pattern to distinguish between collection of patches in Fig.5c and Fig.5d.

The image fragmentation is a well-studied topic and various approaches have been developed to measure the degree of fragmentation (e.g. see [14] and references therein). In our definition of the fragmentation rate we follow paper [11] wherein the definition was taken from the original work [13]. Let $u_b(x, y)$ be the binary image converted from spatial density distribution $u(x, y)$ as follows

$$u_b(x, y) = 1 \quad \text{for} \quad u(x, y) > 0, \quad u_b(x, y) = 0 \quad \text{for} \quad u(x, y) = 0. \tag{16}$$

Fragmentation rate $I_{fr}(u_b(x,y))$ is then defined as

$$I_{fr}(u_b) = 1 - \frac{s(u_b)}{B[p(u_b)]}, \tag{17}$$

where $p(u_b)$ is the population density calculated for the 'binary' population, $s(u_b)$ is a degree of fragmentation for a given population u_b and is related to the average number of neighboring objects in the population image, and $B[p(N_b)]$ is the maximum possible value of the index $s(N_b)$ among all distributions N_b with a given abundance $p(N_b)$; see [11] for a detailed explanation of formula (17). The fragmentation rate calculated according to (17) is $I_{fr} = 0.40$ for the image in Fig.5c and $I_{fr} = 0.53$ for the image in Fig.5d.

Let us investigate how the fragmentation rate of the image of the spatial pattern depends on parameter m in problem (7-8). As in our computation of the other topological indices, we compute the fragmentation rate I_{fr} for each spatial distribution obtained for $\beta = 0.21$ and $\gamma = 6.0$ at time $t = 600$ when $m \in [0.362, 0.396]$. The graph $I_{fr}(m)$ is shown in Fig. 6b where we assume that $I_{fr} = 0$ corresponds to the extinction regime (i.e. no objects in the spatial domain). It is seen from the graph that the fragmentation rate increases when we decrease parameter m and patchy structures become more distinct. However, although the topological index I_{fr} has been employed to distinguish between various fine spatial structures of patchy patterns, it does not even define accurately the range of parameter m where patchy spatial patterns appear. Random variations in the fragmentation rate may stem from the fact that continuous front spatial patterns have a complex density distribution behind the front (cf. Fig. 3g and Fig. 3h) and therefore images of continuous front patterns and patchy patterns may have similar fragmentation rates.

To conclude this section we note that topological indices allow one to distinguish between various continuous front topological regimes yet we cannot rely upon the topological indices when we want to compare two patchy spatial distributions to each other. Patchy patterns obtained for close values of parameter m (while the other problem parameters remain the same) may have very different topological structures. Our study of graphs in Fig. 4 and Fig. 6 reveals that we cannot predict what transformation the spatial pattern will undergo when we give a small increment to m in the parametric sub-domain corresponding to the formation of patchy spatial distributions.

4 Spatio-temporal patterns: temporal evolution of topological characteristics

Topological properties of spatial patterns studied in the previous sections imply their 'topological stability', i.e. once a certain type of spatial pattern has been established as a result of evolution of initial conditions (9-10) it is not transformed into another topological structure (i.e. patchy pattern to continuous front pattern and vice versa). Meanwhile, the definition of 'topologically stable' spatial pattern requires further discussion. It is obvious that any spatial pattern appears as a continuous front (i.e. the number of objects is $n = 1$) at small times as

$n = 1$ for the initial condition spatial distribution and the impact of initial conditions (9-10) is still strong at small times. Let us define the transition time t^* as the time over which transition from the initial condition to the topologically stable spatial distribution occurs, i.e. if a spatial pattern has a certain topological structure (continuous front or patchy distribution) at time t^*, then the same type of topological structure will remain at a later time $t > t^*$. A continuous front spatial structure at small times can evolve into a patchy spatial pattern over the time interval $t \in [0, t^*]$ and it will then remain patchy at $t > t^*$. However, the evolution from continuous spatial structure to a patchy one is not monotone, as multiple switches between continuous front and patchy spatial patterns can be observed at $t < t^*$. Furthermore, spatial structures that are classified as continuous fronts after the transition time show similar behaviour with multiple transformations back and forth to patchy distributions before the end of the transient regime.

Consider, for example, line $\beta = 0.22$ in the parametric plane of Fig. 2b. One simple illustration of the transient spatio-temporal dynamics is shown in Table 1 where we compare spatial patterns that appear at time $t = 300$ and $t = 600$. It is seen from the table that spatial patterns we have at time $t = 300$ are not topologically stable: a patchy spatial structure observed at time $t = 300$ for $m = 0.399$ evolves into a continuous front at $t = 600$, while a continuous front at $t = 300$ for $m = 0.398$ becomes a patchy spatial distribution at $t = 600$. Our numerical tests reveal that similar transient dynamics are observed for other values of m and β in the parametric plane.

m	≤ 0.386	$0.387 \leq m \leq 0.395$	0.396	0.397	0.398	0.399	≥ 0.400
$N_{t=300}$	e	p	p	c	c	p	c
$N_{t=600}$	e	p	c	c	p	c	c

Table 1: *Comparison of spatial patterns for $\beta = 0.22$, $\gamma = 6.0$ and various m at times $t = 300$ and $t = 600$. The legend in the table is as follows: e - extinction, p - patchy spatial distribution, c - continuous front spatial distribution; see also Fig. 2b. Spatial distributions are not topologically stable as switches between continuous front and patchy structures are observed.*

Given the volatile spatio-temporal dynamics in the table, our next goal is to evaluate the transition time t^* to conclude about the topological stability of a given spatial pattern. The empirical study of time t^* in the model (3–4) has been attempted in [19] where the transition time has been evaluated as $100 < t^* < 300$. In the present paper, we further investigate this issue and we use information about the number of objects n in a spatial pattern as we aim for a more accurate evaluation of the transition time. In the computational routine, we employ for this purpose the spatio-temporal dynamics is traced over time T, where we assume that $T \gg t^*$, and the number of objects n is recorded at every time $t_{k+1} = t_k + \Delta t$, $k = 1, \cdots, K-1$ to form the dataset $n(t_k)$ (see Fig. 7). We define the simple topological index I_t of the spatial distribution at given time t_k, $k = 1, \cdots, K$ as $I_t = 0$ if we have extinction regime at time t_k (i.e. $n(t_k) = 0$). We also define $I_t = 1$ for continuous front pattern ($n(t_k) = 1$) and $I_t = 2$ for patchy pattern ($n(t_k) > 1$). The number of objects in the dataset $n(t_k)$ is then replaced by

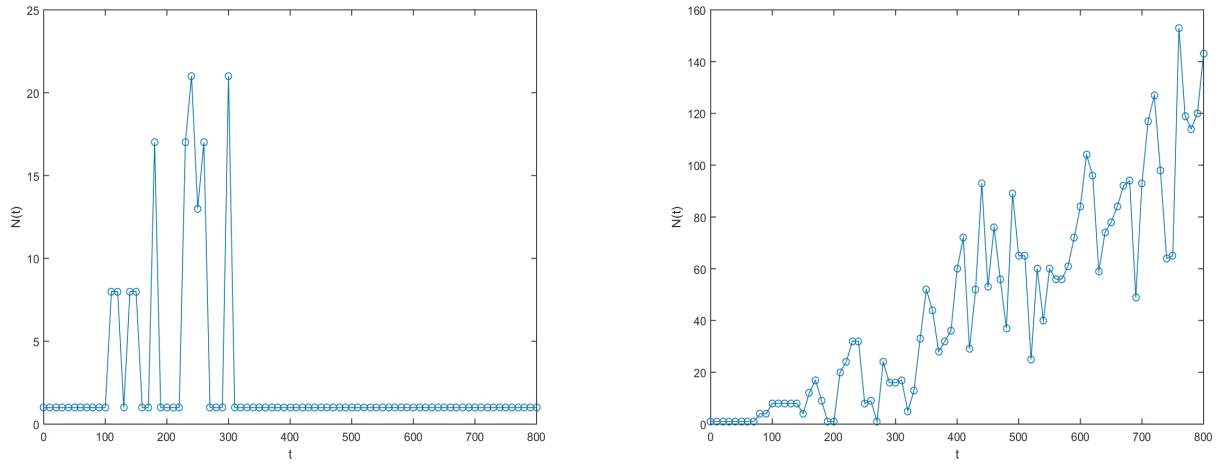

(a) (b)

Figure 7: *The number of objects n as a function of time t for spatio-temporal dynamics with $\beta = 0.21$ and $\gamma = 6.0$: (a) $m = 0.381$: convergence to continuous front spatio-temporal dynamics, $n(t) = 1$ at any time $t > t^* = 310$ (b) $m = 0.374$: convergence to patchy spatio-temporal dynamics; $n(t) > 1$ at any time $t > t^* = 280$.*

index $I_t(k)$. The most straightforward way[3] to define transition time t^* is to find number k^* that satisfies condition $i(k) = i(K)$ for any $k > k^*$. Given k^*, transition time t^* is evaluated as $t^* = k^* \Delta t$.

Consider Fig. 7 where the number of objects is shown as a function of time for spatio-termporal dynamics defined by parameters $\beta = 0.21$, $\gamma = 6.0$ and we have $m = 0.381$ in Fig. 7a and $m = 0.374$ in Fig. 7b. It is readily seen from the graph in Fig. 7a that spatial patterns appear as a continuous front ($n = 1$) at any time $t > t^* = 310$, while spatial patterns are not topologically stable (i.e. the number of objects varies) at times $t < t^*$. Examples of topologically different spatial distributions before transition time t^* are shown in Fig. 8a and Fig. 8b. Similarly, the analysis of Fig. 7b reveals that it is always a patchy spatial pattern for time $t > t^* = 280$ while occasional transitions to a continuous front appear at $t < t^*$; see also examples of spatial distributions in Fig. 8c and Fig. 8d. We would like to emphasise here that both continuous front and patchy spatio-temporal dynamics may experience switches between the two regimes when time $t < t^*$; this is contrary to the conclusion in [19] where it was suggested that only a continuous front regime may exhibit topological instability at $t < t^*$.

[3]We note, however, that more sophisticated filtering algorithms can be employed to find time t^*; e.g. see [38].

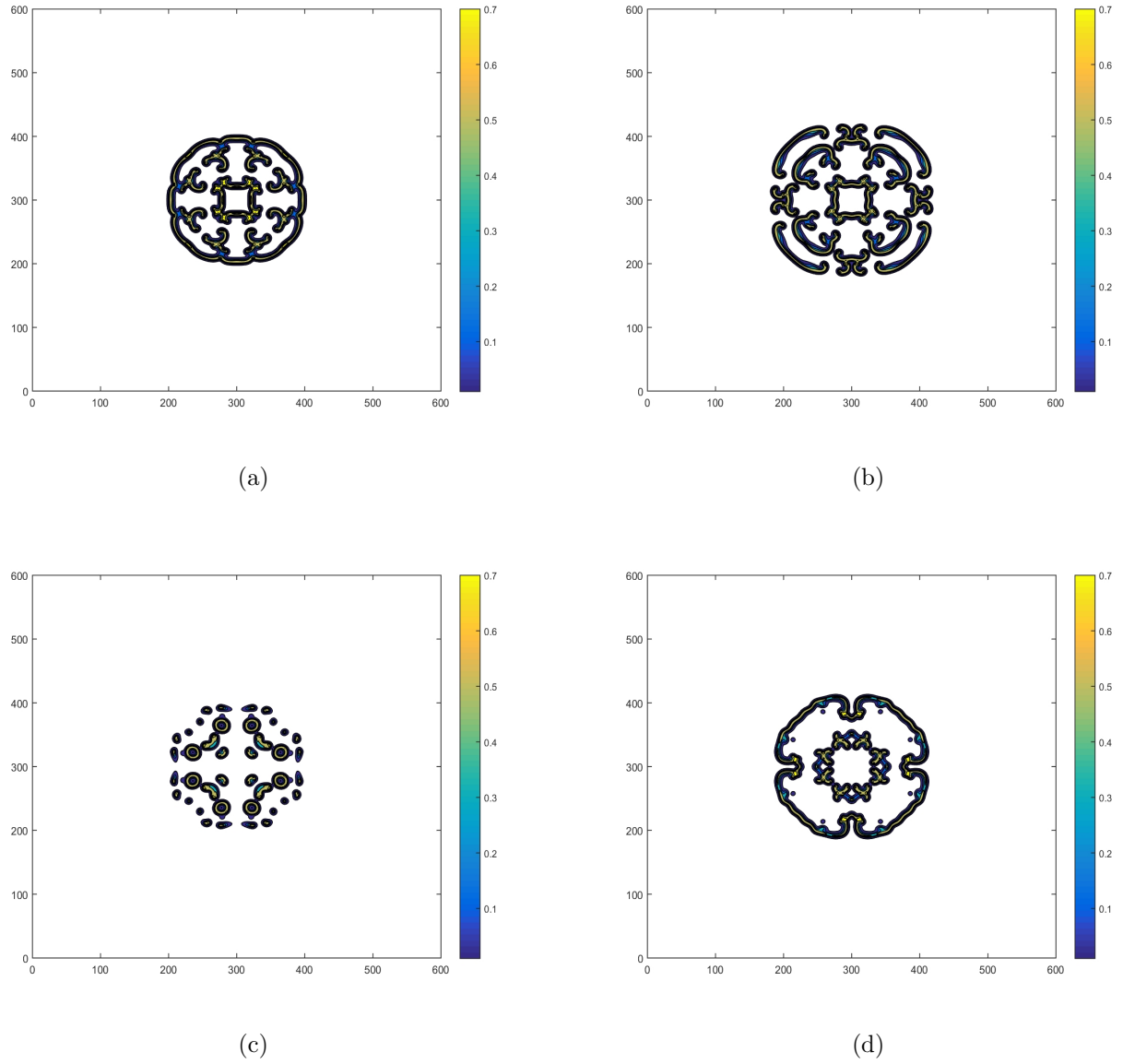

Figure 8: *Examples of occasional switches between patchy and continuous front spatial distributions over transition period* $0 < t < t^*$. *The system parameters are as in Fig. 7. (a)-(b) The spatio-temporal dynamics of Fig. 7a, the transition time to the continuous front spatial pattern is* $t^* = 310$. *(a) continuous front pattern at time* $t_1 = 200 < t^*$, *(b) patchy pattern at time* $t_2 = 250$ *where* $t_1 < t_2 < t^*$; *(c)-(d) The spatio-temporal dynamics of Fig. 7b, the transition time to the patchy spatial pattern is* $t^* = 280$. *(c) patchy pattern at time* $t_1 = 230 < t^*$, *(d) continuous front pattern at time* $t_2 = 270$ *where* $t_1 < t_2 < t^*$;

4.1 Topological stability of invasion regimes

It immediately follows from the example presented in Fig. 7 that transition time t^* depends on the system parameters m, β and γ. Hence, following our approach in the previous section,

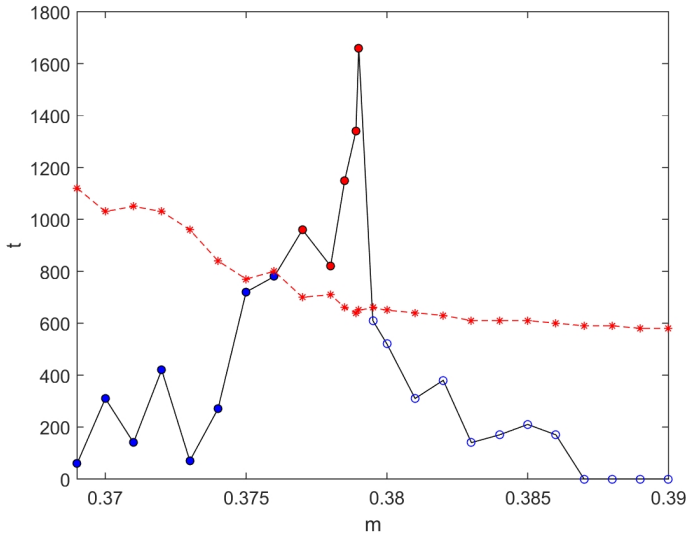

Figure 9: *The transient dynamics of model (7–8) with initial conditions (9–10) and parameters* $\beta = 0.21$, $\gamma = 6.0$. *Transition time* t^* *(solid blue curve, open and closed circles) and time* t^D *required for the invasive species to spread over square domain* D *of linear size* $L = 600$ *(dashed red curve, red stars) are shown as functions of parameter* m. *Open circles on graph* $t^*(m)$ *show time* t^* *required for a transition to continuous front spatio-temporal dynamics, while closed blue and red circles correspond to spatio-temporal dynamics resulting in patchy patterns after* t^*. *For* $m < 0.365$ *transition to extinction happens at* $t^* \approx 50$ *(not shown in the figure). For* $m > 0.386$ *the initial 'continuous front' density distribution given by (9–10) never experiences switches to patchy spatial pattern, i.e.* $t^* = 0$. *Closed blue circles on graph* $t^*(m)$ *show topologically stable spatio-temporal dynamics in domain* D, *while closed red circles show topologically unstable dynamics in* D *(see further explanation in the text).*

we now investigate how time t^* varies when we vary parameter m for $\beta = 0.21$ and $\gamma = 6.0$. The graph $t^*(m)$ is shown as a solid curve in Fig. 9. Every point on curve $t^*(m)$ in the figure presents transition time t^* evaluated according to the procedure described in Section 4 for spatio-temporal dynamics obtained from the evolution of initial condition (9) with a given value of m. Open circles on the curve correspond to the transition to the spatio-temporal dynamics of a propagating continuous front after t^* while closed circles correspond to spatio-temporal dynamics resulting in propagation of patchy spatial patterns after t^*. The analysis of the graph reveals that the following classification of spatial patterns appearing in the system when m is varied can be made for $t > t^*$: the invasive population becomes extinct for $m < 0.365$ (extinction happens at $t^* \approx 50$ for that range of parameter m and the range of m leading to extinction is not shown in the figure for the sake of convenience), the invasive population spreads into space as a collection of separate density patches for $m \in [0.365, 0.379]$, the invasive species propagates as a continuous front with oscillations in the wake for $m \in [0.380, 0.386]$, and the propagating continuous front has no oscillations in the wake for $m > 0.386$ (cf. Fig. 3).

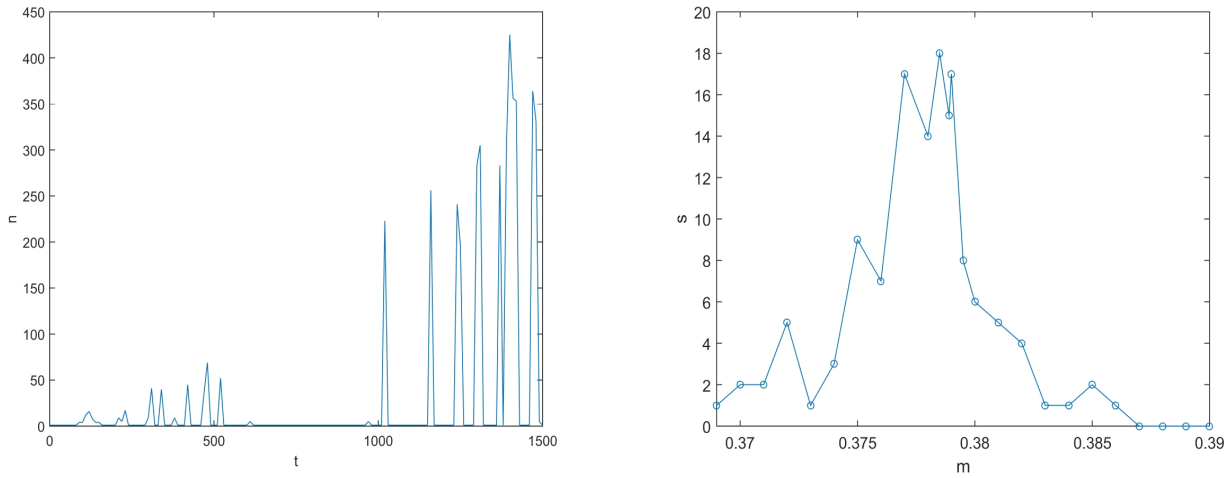

(a) (b)

Figure 10: *(a) Example of multiple random switches between continuous front and patchy spatial distributions. The number of objects n is shown as a function of time $t \in [0, 1500]$ for $m = 0.379$, $\beta = 0.21$, $\gamma = 6.0$. Parameter $m = 0.379$ presents the boundary between patchy and continuous front topological zones. (b) The number of switches s between patchy and continuous front regimes over time $t = 1500$ as a function of parameter m.*

An essential feature of graph $t^*(m)$ is that the range of transition times t^* is much larger when m is taken from 'patchy' topological zone $m \in [0.365, 0.379]$. While time t^* is in good agreement with the estimate made in [19] for spatio-temporal dynamics of continuous fronts arising when m is selected not very close to the boundary of the 'patchy' range (i.e. we have $t^* < 300$ for $m > 0.382$), the maximum transition time we have observed in our computation of patchy spatio-temporal dynamics is $t^* = 1750 \gg 300$ obtained for $m = 0.379$. It also is worth noticing here that for the above-mentioned 'patchy' range of m the number of random switches between patchy and continuous front patterns registered at $t < t^*$ does not decrease as time increases and gets closer to t^*. An example is shown in Fig. 10a where we have recorded all switches between patchy (number of objects $n > 1$) and continuous front ($n = 1$) regimes over time interval $t \in [0, 1500]$ for $m = 0.379$ (we recall that $t^* = 1750$). It is seen from the figure that time $t = 600$ can be erroneously thought of as the transition time t^* as there are no switches at time $t \in [600, 950]$. However, after $t = 950$ random jumps between patchy and continuous front regimes resume. The transitional dynamics is further presented in Fig. 10b where the number of switches s over the same time interval $t \in [0, 1500]$ is shown as a function of m. It is seen from the figure that indeed the largest number of switches occurs when m belongs to the 'patchy' range, $m \in [0.365, 0.379]$.

One important observation about transition time t^* is that in practical consideration it has to be compared to time t^D required for invasive species to spread over the spatial domain D where the species is monitored. Indeed, if we want to identify the invasion regime (continuous

vs. patchy) in some spatial domain D to make an adequate control decision on the invasion prevention, we have to collect reliable information about spatial pattern before domain D will be fully invaded. Hence if $t^* > t^D$ then we cannot give any recommendation on invasion control based on the type of spatial pattern. In other words, we will still have a transient regime at time t^D where we cannot say for sure what spatial pattern we deal with in domain D, while the domain is already completely invaded at $t = t^D$ and it, therefore, is too late to make a control decision.

The time t^D required for invasive species in the model (7-8) to spread over square domain D with linear size L is shown as a function of parameter m for $L = 600$ in Fig. 9; see a dashed red line in the figure. In all cases presented in the figure, computation has been performed in a larger spatial domain where the square domain D has been considered as a sub-domain placed at the center of the computational domain. We do not show time t^D in the graph for extinction regime $m < 0.365$ because the extinction of the invasive species happens at $t^* \approx 50$, i.e. well before domain D becomes fully invaded. It is seen from the figure that for continuous front regimes with $m > 0.379$ the transition time is always $t^* < t^D$. The conclusion about the relationship between t^* and t^D is, however, different when we consider the range of parameter $m \in [0.365, 0.379]$ resulting in patchy spatio-temporal dynamics. We have $t^* > t^D$ for several values of m in the figure. Moreover, transition time $t^*(m)$ is not a monotone function over the interval $m \in [0.365, 0.379]$ and we cannot, therefore, predict what happens to the transition time if m is slightly varied. Thus, if we take an arbitrary value of m from the above interval likely the invasion type cannot be determined in spatial domain D where we are interested in the control of invasive species.

Consider now an arbitrary spatial domain D and let us introduce the ratio

$$r(m) = t^*(m)/t^D(m), \tag{18}$$

where times $t^*(m)$ and $t^D(m)$ are defined as above. For any given value of m, we will say that a spatial pattern is topologically stable in domain D if $r < 1$ and the pattern is topologically unstable in D if $r \geq 1$. The rate r depends on domain size L and we have $r \to 0$ as $L \to \infty$. Meanwhile, another case resulting in $r = 0$ is when transition time is $t^* = 0$, i.e. when the spatio-temporal dynamics does not undergo any switches between patchy and continuous states. We will refer to the latter topological type of spatio-temporal dynamics as unconditionally stable.

Let us apply the above classification to the spatio-temporal dynamics of Fig. 9. The range $m \in [0.365, 0.379]$ resulting in patchy spatio-temporal dynamics can be subdivided as follows: we have topologically stable patchy patterns in domain D for $m \in [0.365, 0.376]$ and topologically unstable 'quasi-patchy' patterns in D for $m \in (0.376, 0.379]$. Meanwhile all continuous front patterns remain topologically stable in D, all of them being unconditionally stable for $m > 0.386$. Hence, we cannot make any conclusion about the topology of spatial pattern in domain D when spatio-temporal dynamics is induced by the demographic parameter $m \in [0.365, 0.376]$, while the topological classification of spatio-temporal patterns obtained for all other values of m can be decided upon before spatial domain D is fully invaded.

The transition time t^* has to be taken into account when the topological indices introduced

in Section 3 are analysed. Consider, for example, the graphs of Fig. 4 and Fig. 6. We recall that all topological indices presented in those figures have been computed for time $\tilde{t} = 600$. Once the transition time has been defined for every spatial pattern whose topological indices are computed, we have $\tilde{t} > t^*$ for continuous front distributions generated when $m > 0.379$. Those spatial patterns are topologically stable (most of them are unconditionally stable) in a spatial domain where the computation has been made. A small increment in parameter m results in a relatively small change of topological properties, i.e. spatial distributions generated for similar values of m will look similar. However, most spatial patterns obtained at time $\tilde{t} = 600$ with m taken from the 'patchy' range have $\tilde{t} < t^*$ and their topologies are not well defined at $t = \tilde{t}$. Hence our next step is to check whether the presence of random oscillations in topological indices is an inherent feature of patchy spatial patterns and those oscillations will not disappear when patchy spatial patterns are analysed at time $t > t^*$.

Several values of the parameter m taken with a small increment from the 'patchy' range are shown in Table 2. For each value of m in the table, the transition time has been defined and we have then selected the maximum value t^*_{max} from the range of transition times. In our computation we had $t^*_{max} = 790$ and spatial patterns have therefore been analysed at time $t = 810 > t^*_{max}$ to ensure that all spatial patterns obtained at that time are already topologically stable. The topological indices of spatial patterns generated at time $t = 810$ are compared to the topological indices calculated for the same range of m at time $t = 600$ in the table.

m	0.3750	0.3752	0.3754	0.3756	0.3758	0.3760
n, $t = 600$	37	1	89	105	89	84
n, $t = 810$	181	115	133	152	142	193
$d \times 10^{-4}$, $t = 600$	8.0	7.0	10.0	15.0	12.0	10.0
$d \times 10^{-4}$, $t = 810$	12.0	9.0	10.0	11.0	12.0	15.0
$I_{fr} \times 10^{-2}$, $t = 600$	4.97	4.83	5.08	5.62	5.52	5.18
$I_{fr} \times 10^{-2}$, $t = 810$	5.17	5.27	5.15	5.37	5.30	5.77
I_M, $t = 600$	3.20	3.36	3.20	3.25	3.45	3.26
I_M, $t = 810$	1.78	2.25	2.23	1.97	2.03	2.06

Table 2: *Topological indices of spatial patterns as a function of parameter m in the model (7)–(8) with the initial conditions (9)–(10) and parameters* $\beta = 0.21$, $\gamma = 6.0$. *The values of m taken with a small increment at the interval* $m \in [0.375, 0.376]$ *result in patchy spatio-temporal dynamics after transition time* t^*. *The number of objects n, the density of objects d, the Morisita index* I_M, *and the fragmentation rate* I_{fr} *are compared at time* $t = 600 < t^*$ *and* $t = 810 > t^*$.

It is seen from the table that irregular variations in the topological indices persist as spatio-temporal dynamics of invasive species is generated by parameter m taken from the 'patchy' sub-domain. A small increment in m still results in random fluctuations in all topological indices even after the topological type of spatial pattern has been established at time $t > t^*$. Random oscillations in the topological indices make a comparison of patchy patterns observed at any fixed moment of time difficult, as spatial distributions obtained for close values of

system parameters may have very different topological indices.

5 Conclusions and discussion

In the present paper, we have discussed how to recognise and compare various spatial patterns arising in the problem of biological invasion. The question of distinguishing between continuous and discontinuous (patchy) spatial distributions has been of particular interest as it is closely related to the problem of monitoring and control of invasive species. On the one hand, timely recognition of 'no front' patchy invasion regimes is important as its monitoring may require more careful resource allocation than monitoring of continuous front spatial distributions. The grid of sampling locations used in the monitoring of discontinuous spatial patterns must be fine enough to capture sufficient information about the population distribution (e.g. see [41, 42]). It has been argued in [41] that patches with the nonzero population density will be partially or completely missed if the distance between sampling locations is greater than the patch size. On the other hand, once a discontinuous spatial pattern has been accurately identified, its control may only require practitioners to deal with the areas occupied by separate density patches and more targeted means of control may, therefore, be applied to prevent the spatial spread of invasive species.

Our study of spatial patterns has been based on results of a mathematical model which is capable of producing a variety of spatial distributions depending on the model parameters. Basic topological characteristics of spatial pattern such as the number of objects, the density of objects, the degree of aggregation (as given by the Morisita index), and the fragmentation rate have been employed to analyse spatial distributions arising in the model. We have checked whether the spatial pattern type can be recognised correctly and two spatial patterns can be compared to each other by using the topological indices above. It has been confirmed in the paper that topological indices allow one to distinguish between various continuous front topological regimes. Meanwhile, our study has revealed that those indices are not reliable when we want to compare two 'no front' patchy spatial distributions as patchy patterns that look similar to each other may have very different topological indices. Hence, we have further studied how the topological indices used to quantify spatial patterns respond to a change in the model parameters. It has been argued in the paper that close parameter values generate spatial distributions with similar topological indices when the simple topology of a continuous front is considered. However, there is no clear link between the model parameters and the topological indices when we deal with complex topological structures such as continuous front density distributions with patches behind the front or patchy distributions that do not form a continuous propagation front. One important observation is that transition from continuous front spatial patterns to 'no front' patchy spatial distributions as model parameters vary does not result in any distinct and predictable change in the density of objects, the Morisita index, and the fragmentation rate, although the number of objects provides us with a correct answer about the topological type of spatial pattern.

In our attempt to explain random fluctuations of topological indices observed when close

values of the system parameters are considered we have investigated spatio-temporal dynamics of the invasive species to see whether those fluctuations will disappear as time progresses. Our study of the temporal evolution of spatial patterns resulted in the conclusion that, along with the topological indices, transition time t^* required for 'topological stabilisation' of spatial patterns must be taken into account. If a spatial pattern is considered at time $t < t^*$ its topological properties may significantly change with time, i.e. continuous front spatial pattern may transform itself into a patchy pattern and vice versa. Thus, spatial patterns can only be identified after transition time t^* and it appears that the transition time can be much greater for patchy invasion regimes than for continuous front regimes. Moreover, it has been found in the paper that for spatio-temporal dynamics resulting in the formation of patchy patterns the transition time can also be much greater than time t^D required for the invasive species to spread over some spatial domain D where invasive species are monitored. The latter case is true for most patchy regimes considered in the paper and those regimes have been labelled as 'topologically unstable' in domain D. By the definition of topologically unstable patterns their topological type cannot be determined in domain D where we want to control the spread of invasive species.

Our study reveals that propagation of patchy density distributions present the most difficult case of the spatio-temporal dynamics of invasive species when topological properties of spatial distribution have to be determined. It has been argued in the paper that patchy spatial patterns obtained for close values of system parameters may have very different topological structures even after the transition time and we, therefore, cannot rely upon the topological indices if two patchy spatial distributions are compared to each other. We notice here that persisting irregular variations in topological indices may indicate that we have chaotic spatio-temporal dynamics when propagation of invasive species results in formation of patchy spatial patterns in invaded areas. A well-informed conclusion about chaotic dynamics requires us to study the sensitivity of model (7-8) to a perturbation of the initial conditions (e.g. see [37, 59]) and, while the investigation of this issue is beyond the scope of the present paper, it will consist the topic of future work.

We would like to emphasise here that, according to the results in Section 4, registration of separate patches at any time $t < t^*$ cannot serve as a reliable indicator of patchy invasion as separate patches can be transformed into a continuous front after the transition time. Thus, another conclusion of our study is that timely recognition of patchy invasion regimes may be a challenging issue that may require allocation of additional monitoring resource and therefore determination of reliable 'early signs' of patchiness should consist another topic of future work.

The results of our study are problem-specific, yet our approach to the analysis of spatial patterns can be readily extended to spatial distributions produced as the result of a different model. Meanwhile, reliable identification of topological properties of patchy patterns may require the implementation of more advanced methods of spatial analysis as well as the development of novel techniques of pattern recognition and comparison. Those techniques should, in turn, be based on a clear understanding of the spatio-temporal dynamics of patchy invasion regimes when a certain mathematical model is employed for simulation of spatial data. Establishing the solid link between topological quantities used for characterization of spa-

tial pattern and controlling parameters in the model should help researchers with answering the key question of whether the underlying process can be predicted from analysis of spatial pattern.

6 Acknowledgments

The authors thank John Ellis and Simran Sandhu for their careful reading of the manuscript. Helpful comments made by two anonymous referees are gratefully acknowledged.

References

[1] Amaral, M.K., Pellico Netto, S., Lingnau, C., Figueiredo Filho, A. (2015) Evaluation of the Morisita index for determination of the spatial distribution of species in a fragment of araucaria forest. Appl. Ecol. Environm. Res. 13(2):361-372

[2] Britton, N. F. (2003) Essential Mathematical Biology. New York, NY: Springer.

[3] Cressie, N. (1993) Statistics for Spatial Data. John Wiley and Sons, New York, New York, USA, 921 pps.

[4] Dale, M.R.T., Dixon, Ph., Fortin, M.-J., Legendre, P., Myers, D.E. & Rosenberg, M.S. Conceptual and mathematical relationships among methods for spatial analysis. Ecography, 25: 558–577

[5] Dale, M., Fortin, M. (2014) Spatial analysis: A Guide for Ecologists. Cambridge University Press, UK, 365 pps.

[6] Dennis, B. (1989) Allee effects: population growth, critical density, and the chance of extinction. Natural Resources Modeling, 3:481–53

[7] Ellis, J.R., Petrovskaya,N.B., & Petrovskii, S.V. (2019) Effect of density-dependent individual movement on emerging spatial population distribution: Brownian motion vs Levy flights. Journal of Theoretical Biology, 464:159178

[8] Fang, W. (2005) Spatial analysis of an invasion front of Acer platanoides : dynamic inferences from static data. Ecography, 28: 283–294

[9] Fisher, R.A. (1937) The wave of advance of advantageous genes. Ann. Eugen. 7:355-369

[10] Fortin, M.-J. (2017) Spatial analysis of ecological data. in: S. Shekhar et al. (eds.), Encyclopedia of GIS, Springer, 1949–1957

[11] Garnier, G., Roques, L., & Hamel, F. (2012) Success rate of a biological invasion in terms of the spatial distribution of the founding population. Bull. Math. Biol., 74:453-473

[12] Grimm, V. (1994) Mathematical models and understanding in ecology. Ecol. Model., 75/76:641–651

[13] Harary, F. & Harborth, H. (1976) Extremal animals. Journal of Combinatorics, Information and System Sciences 1:1–8

[14] Hargis, C.D., Bissonette, J.A., & David, J.L. (1998) The behavior of landscape metrics commonly used in the study of habitat fragmentation. Landscape Ecology, 13:167–186

[15] Hayes, J.J., Castillo, O. (2017) A new approach for interpreting the Morisita index of aggregation through quadrat size. Int. J. Geo-Inf. 6, 296; doi:10.3390/ijgi6100296

[16] Hutchinson, G.E. (1953) The concept of pattern in ecology. Proceedings of the Academy of Natural Sciences of Philadelphia, 105:1-12

[17] Hui C., Veldtman R. and McGeoch, M.M. (2010) Measures, perceptions and scaling patterns of aggregated species distributions. Ecography 33:95-102

[18] Hurlbert, S. (1990) Spatial distribution of the montane unicorn. OIKOS 58:257271

[19] Jankovic, M., & Petrovskii, S.V. (2013) Gypsy moth invasion in North America: a simulation study of the spatial pattern and the rate of spread. Ecol. Compl. 14:132-144

[20] Jeltsch, F., Moloney, K. & Milton, S. J. (1999) Detecting process from snapshot pattern: lessons from tree spacing in the southern Kalahari. Oikos 85:451–466

[21] Kanevski, M. (2004) Analysis and Modelling of Spatial Environmental Data. EPFL Press: Lausanne, Switzerland.

[22] Kolmogorov, A.N., Petrovskiy, I.G., Piskunov, N.S. (1937) A study of the diffusion equation with increase in the quantity of matter, and its application to a biological problem. Bull. Moscow Univ. Math. Ser. A 1:1-25

[23] Legendre, P. & Fortin, M.J. (1989) Spatial pattern and ecological analysis. Vegetatio, 80: 107–138

[24] Levin, S.A. (1992) The problem of pattern and scale in ecology. Ecology 73: 1943–1967

[25] Lewis, M.A., Kareiva, P. (1993) Allee dynamics and the spread of invading organisms. Theoretical Population Biology 43:141–158

[26] Lewis, M.A., Petrovskii, S.V., & Potts, J. (2016) The Mathematics Behind Biological Invasions. Interdisciplinary Applied Mathematics, Vol. 44. Springer.

[27] Liebhold, A.M., Elmes, G.A., Hawerson, J.A., Quimby, J. (1994) Landscape characterization of forest susceptibility to gypsy moth defoliation. Forest Science 40:18–29

[28] Liebhold, A.M., Bascompte, J. (2003) The Allee effect, stochastic dynamics and the eradication of alien species. Ecology Letters 6:133–140

[29] Liebhold, A.M., Gurevitch, J. (2002) Integrating the statistical analysis of spatial data in ecology. Ecography 25:553–557

[30] https://uk.mathworks.com/help/images/index.html

[31] McIntire, E. J. B., & Fajardo, A. (2009) Beyond description: the active and effective way to infer processes from spatial patterns. Ecology 90: 46–56

[32] Mistro, D.C., Rodrigues, L.A.D. & Petrovskii, S.V. (2012) Spatiotemporal complexity of biological invasion in a space- and time-discrete predator–prey system with the strong Allee effect. Ecol. Compl. 9:16–32

[33] Morisita, M. (1959) Measuring of the dispersion of individuals and analysis of the distributional patterns. Mem. Fac. Sci. Kyushu Univ. Ser. E 3:65–80

[34] Morozov, A.Y., Petrovskii, S.V. & Li, B.L. (2006) Spatiotemporal complexity of patchy invasion in a predator-prey system with the Allee effect. J. Theor. Biol. 238:18–35

[35] Murray, J. D. (2002) Mathematical Biology I: an Introduction. New York, NY: Springer.

[36] Murray, J. D. (2003)Mathematical Biology II: Spatial Models and Biomedical Applications. New York, NY: Springer.

[37] Nayfeh, A.H., Balachandran, B. (1995) Applied Nonlinear Dynamics. New York: Wiley.

[38] Oppenheim, A. V., Schafer, R. W., & Buck, J.R. (1999) Discrete-Time Signal Processing. Upper Saddle River, NJ: Prentice-Hall.

[39] Perry, J.N. (1995) Spatial analysis by distance indices. Journal of Animal Ecology 64: 303-314

[40] Perry, J. N., Liebhold, A.M., Rosenberg, M.S., Dungan, J., Miriti, M., Jakomulska. A., CitronPousty, S. (2002) Illustrations and guidelines for selecting statistical methods for quantifying spatial pattern in ecological data. Ecography, 25: 578–600

[41] Petrovskaya, N.B., Embleton, N.L. (2013) Evaluation of peak functions on ultra-coarse grids. Proceedings of the Royal Society A 469: 20120665 doi: 10.1098/rspa.2012.0665

[42] Petrovskaya, N.B., Petrovskii, S.V. (2010) The coarse-grid problem in ecological monitoring. Proceedings of the Royal Society A 466:2933–2953

[43] Petrovskaya, N.B., Petrovskii, S.V. & Zhang, W. (2017) Patchy, not patchy, or how much patchy? Classification of spatial patterns appearing in a model of biological invasion. Math. Model. Nat. Phenom., 12:208-225

[44] Petrovskaya, N.B. & Zhang, W. (2019) Accurate recognition of spatial patterns arising in spatio-temporal dynamics of invasive species. in: in: M.Aguiar, C.Braumann, B.Kooi, A.Pugliese, N.Stollenwerk, E.Venturino (eds.), Current Trends in Dynamical Systems in Biology and Natural Sciences, SEMA-SIMAI Springer Series, Springer, Berlin (accepted for publication)

[45] Petrovskii, S.V., Morozov, A.Y. & Venturino, E. (2002) Allee effect makes possible patchy invasion in a prey-predator system. Ecol. Lett. 5:3450-352

[46] Petrovskii, S.V., Petrovskaya, N.B. & Bearup, D. (2014) Multiscale approach to pest insect monitoring: random walks, pattern formation, synchronization, and networks. Physics of Life Reviews 11:467-525

[47] Petrovskii, S.V., Malchow, H., Hilker, F.M. & Venturino, E. (2005) Patterns of patchy spread in deterministic and stochastic models of biological invasion and biological control. Biological Invasions 7:771-793

[48] Pielou, E. C. (1977) Mathematical ecology. John Wiley and Sons, Inc., Hoboken, NJ

[49] Rodrigues, L.A.D., Mistro, D.C. & Petrovskii, S.V. (2012) Pattern formation in a space- and time-discrete predator–prey system with a strong Allee effect. Theor. Ecol. 5:341-362

[50] Rodrigues, L.A.D., Mistro, D.C., Petrovskaya, N.B. & Petrovskii, S.V.(2015) Patchy invasion of stage-structured alien species with short-distance and long-distance dispersal. Bulletin of Mathematical Biology, 77:1583-1619

[51] Rosenberg, M. & Anderson, C. (2016) Spatial Pattern Analysis. In: Oxford Bibliographies in Ecology (ed David Gibson). NY: Oxford University Press.

[52] Sharov, A.A. and Liebhold, A.M. (1998) Model of slowing the spread of gypsy moth (Lepidoptera: Lymantridae) with a barrier zone. Ecological Applications 8:1170-1179

[53] Sherratt, J.A., Lewis, M.A., Fowler, A.C. (1995) Ecological chaos in the wake of invasion. Proc. Natl. Acad. Sci. U. S. A. 92:25242528

[54] Sherratt, J.A., Smith, M.J. (2008) Periodic travelling waves in cyclic populations: Field studies and reactiondiffusion models. J. R. Soc. Interface 5:483505

[55] Shigesada, N., Kawasaki, K. (1997) Biological Invasions: Theory and Practice. Oxford: Oxford University Press.

[56] Shigesada, N., Kawasaki, K and Takeda,Y. (1995) Modelling stratified diffusion in biological invasions. Amer. Nat. 146, 229-251.

[57] Skellam, J.G. (1951) Random dispersal in theoretical populations. Biometrika 38:196-218

[58] Sosa, B., Romero, D., Fernndez, G., & Achkar, M. (2018) Spatial analysis to identify invasion colonization strategies and management priorities in riparian ecosystems. Forest Ecology and Management, 411: 195–202

[59] Strogatz, S.H. (2000) Nonlinear Dynamics and Chaos: With Applications to Physics, Biology, Chemistry and Engineering. Reading MA: Perseus Books.

[60] Wittenberg, R., Cock, M.J.W. (eds.) (2001) Invasive Alien Species: a Toolkit of Best Prevention and Management Practices. CAB International, Wallingford, Oxon, UK, xvii - 228